IOP Publishing Superconductor Science and Technology
Supercond. Sci. Technol. 31 (2018) 075010 (8pp) https://doi.org/10.1088/1361-6668/aac860

Lateral motion stability of high-temperature superconducting maglev systems derived from a nonlinear guidance force hysteretic model

Haitao Li[1], Zigang Deng[1,3], Li'an Jin[1,2], Jipeng Li[1], Yanxing Li[1] and Jun Zheng[1]

[1] Applied Superconductivity Laboratory, State Key Laboratory of Traction Power, Southwest Jiaotong University, Chengdu 610031, People's Republic of China
[2] School of Mechanics and Engineering, Southwest Jiaotong University, Chengdu 610031, People's Republic of China

E-mail: deng@swjtu.cn

Received 31 January 2018, revised 14 May 2018
Accepted for publication 29 May 2018
Published 12 June 2018

Abstract

High-temperature superconducting (HTS) maglev, owning to the capability of passive stabilization, is potentially promising for high-speed transportation. The guidance force of bulk HTS materials above a permanent magnetic guideway has a nonlinear response due to the hysteresis effect. As a kind of rail transit, when the vehicle runs along the track, the curve and other disturbances will cause vibrations to the vehicle system. These physical factors will pose dynamic loads on the components, reducing structural reliability as well as affecting the ride comfort. The lateral motion, as an important part of the vehicle system dynamics, needs to be studied in the pursuit of HTS maglev realization. In this paper, we first measured the guidance forces of HTS bulks under different motion conditions, and analyzed the relationship between the lateral displacement, the movement velocity and the guidance force. Then, a mathematical model was built based on these experimental data. The key feature of this mathematical model is that it can describe the hysteresis characteristic of the guidance force. Based on this model, we investigated the lateral motion stability of the HTS levitation system, and found three singular points, one stable focus point, and two unstable saddle points. Lastly, a phase portrait was proposed to indicate the safe working region of the HTS maglev vehicle where the vehicle can automatically return to its equilibrium position. These experimental and simulation results are important to clarify the lateral motion stability under external disturbance or shock, and provide a reference basis for the design of levitation systems.

Keywords: HTS maglev, lateral motion, simulation calculation, guidance force, nonlinear hysteretic model

(Some figures may appear in colour only in the online journal)

1. Introduction

Bulk high-temperature superconductors (HTSs) possess an extraordinary flux pinning property which enables them to levitate, passively stable, above a permanent magnetic guideway (PMG) [1]. This newly emerged levitation technology has attracted the attention of researchers worldwide [2–5]. As a rail transit system, the vehicle was restricted to the transit lines mainly by the levitation and guidance force between HTS bulks and the PMG, making the HTS/PMG relation the core of the vehicle/track system. Therefore, the lateral motion stability and the curve negotiation ability has become the main research

[3] Author to whom any correspondence should be addressed.

focus regarding the vehicle dynamics, and the motion stability is the key issue in the design and safe operation of HTS maglev systems [6, 7]. In this field, researchers have focused on the static and quasi-static mechanical characteristics of the interaction between HTS bulks and permanent magnets (PMs) [8–11]. Moon *et al* noted hysteresis when measuring the guidance force [8], and the quasi-periodic vibration was further experimentally investigated by Hikihara [9]. Soon after, numerical simulation was also used to study the stability of the HTS maglev system. As a unique phenomenon of the HTS maglev system, when the HTS bulk is moved laterally, a restoring force will be generated to attract it back to its equilibrium position, which is called 'self-stable' [1]. If this displacement is large enough, the restoring force is transformed from elastic deformation to elastic−plastic deformation, and consequently the HTS bulks can no longer return it to its equilibrium position. When the lateral displacement of the bulk superconductor exceeds a certain limit, the guidance force starts to decrease with the increasing displacement, and the lateral motion of the vehicle becomes unstable [12]. This means the 'self-stable' property of the HTS maglev system is based on the hysteretic restoring force between the HTS bulks and the PMG [1], and the 'stability' is conditional. For instance, the thermally activated flux creep in the HTS bulks not only results in the relaxation of the levitation force [13], but also leads to the dynamic drift of the levitated object [14], which is closely related to the localized and short-term dynamic stability of the HTS maglev system. Hence, the HTS maglev system is a typical nonlinear system due to the flux instability. The nonlinear hysteretic nature of the HTS−PM interaction is believed to be the main cause of the complicated dynamic behaviors [15]. Studies on the linear and nonlinear dynamic behavior of the HTS maglev system have been reported, and most of these studies paid attention to vertical vibrations [9–11, 13–20]. However, only few of them discussed lateral vibration, one of the main research topics in the dynamics of such vehicles [19].

The dynamic response of the vehicle system is caused by the orbital incentive and dynamic load transmitted via the magnetic forces. Changes to these loads can affect the comfort, stability and safety of the vehicle. Therefore, it is necessary to establish a reliable model regarding the magnetic force to study the dynamic response of the vehicle system. Some papers have used critical state or power law models to model the hysteretic force of the HTS maglev system [19, 21, 22]. These models are usually solved by numerical algorithms such as the finite element method, and are not widely used in dynamics analysis because of the limitation of the computing speed. So, in such dynamics, researchers try to describe the levitation and guidance force using fitted mathematical models. The relationship between the levitation force and gap is almost clear after years of research [9, 15, 23]; however, no guidance force model has been reported yet. The guidance force is dependent not only on the relative displacement but also on the velocity of the relative movement which determines the change of the external field and in turn the shielding current induced within the bulk superconductor during the relative movement. Ma *et al* have reported a numerical study on this phenomenon [19]. However, the hysteretic character of the guidance force in terms of the motion

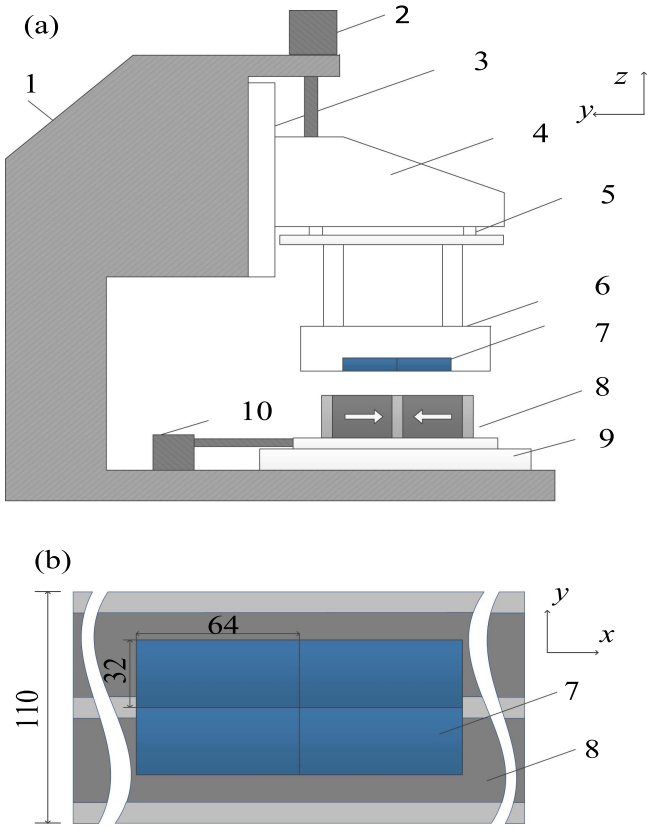

Figure 1. (a) Sketch of the experimental device measuring the guidance force of the HTS bulks: 1—base platform, 2—vertical servomotor, 3—vertical guideway, 4—cantilever, 5—guidance force sensor, 6—liquid nitrogen vessel, 7—YBaCuO bulk superconductors (2 × 2), 8—PMG, 9—horizontal bench, 10—horizontal servomotor. (b) Top view of the YBaCuO bulk superconductors (blue) and the PMG (gray).

velocity has not been measured systematically so far. Following this part, we first reported the measurement of the guidance force (the force between HTS and PMG in the transverse direction) of bulk superconductors above a PMG, to make clear the relationship between guidance force and movement velocity. After that, based on the experimental data, a nonlinear hysteretic model was proposed to describe the guidance force and its hysteretic character. In fact, the hysteretic interaction between the HTS bulks and PM, which comes from the strong flux pinning effect in HTS bulks, is usually the primary cause of nonlinear dynamic behaviors. So, the transverse HTS/PMG relation was applied to investigate the lateral stability of a prototype HTS maglev vehicle. A phase portrait, based on the simulation results, was formulated to describe the local stability of lateral motion. This work is helpful to clarify the lateral motion under external disturbance or shock, and provides a reference basis for the design of levitation systems, which helps in improving the comfort and stability of maglev transit.

2. Experiments

2.1. Experimental setup and procedure

Figure 1(a) shows the schematic diagram of the measurement device [23]. Four 64 mm × 32 mm × 12 mm multi-seeded

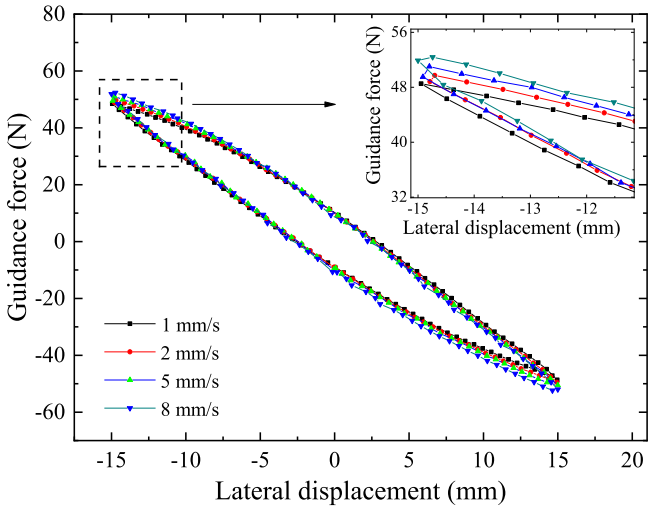

Figure 2. Guidance force versus lateral displacement curve of HTS bulks with various movement velocities above the PMG.

Table 1. Maximum guidance forces of the bulk superconductors at different moving velocities at a lateral displacement of 15 mm and its growth rate using moving velocity of 1 mm s^{-1} as reference.

Velocity (mm s^{-1})	1	2	5	8
Maximum guidance force (N)	48.5	49.7	51.0	52.4
Growth rate		2.7%	5.2%	8.0%

rectangular YBaCuO bulk superconductors, made by ATZ GmbH, Germany, were fixed in a liquid nitrogen vessel (figure 1(a)), and placed above the PMG. The bulk superconductors were kept in the same position in every measurement. A unimodal PMG, 110 mm in width and 50 mm in height and made of NdFeB permanent magnets and steel yokes, was employed to generate the external magnetic field. The vertical component of the flux density has only one peak, at the center.

The experiments were all conducted in field cooling (FC) conditions. The HTS bulks were slowly cooled in a polystyrene liquid N_2 container at a height of $z = 30$ mm [11] in the external magnetic field, and were moved downwards to the lowest position $z = 15$ mm after 15 min. Once reaching the lowest position, the bulk superconductors were returned to their initial position. This process was repeated three times, to ensure a sufficient relaxation in every experiment. After that, the guidance force acting on the HTS bulk superconductors was measured and recorded using the force transducer when the PMG was moved laterally (y-axis) by a designed servomotor. The velocity of the lateral movement of the PMG was selected from 1 mm s^{-1} to 8 mm s^{-1}, with a displacement precision of ±0.1 mm. The transducer used has a precision of ±0.2 N.

2.2. Experimental results and discussion

2.2.1. Guidance force versus lateral movement velocity. Figure 2 shows the hysteresis loops of the guidance force measured with the lateral movement velocity of the PMG set to be 1 mm s^{-1}, 2 mm s^{-1}, 5 mm s^{-1} and 8 mm s^{-1}. The maximum displacement was ±15 mm. By comparing the guidance force curves, it is found that the guidance force is slightly larger when the PMG moves at a higher velocity. This is because the magnetic force is determined by the external field and the shielding current induced in the bulk superconductor during the motion. The external field that works on the bulk superconductor changes faster with a larger lateral moving velocity, which increases the induced shielding current, thus enhancing the magnetic force [19].

Table 1 lists the guidance force values at the maximum lateral displacement of 15 mm to compare the guidance force between different velocities in detail. The maximum guidance forces are 48.5 N, 49.7 N, 51.0 N and 52.4 N, corresponding to movement velocities of 1 mm s^{-1}, 2 mm s^{-1}, 5 mm s^{-1} and 8 mm s^{-1}. Compared with the guidance force at movement velocity of 1 mm s^{-1}, there is a 2.7% increase of the guidance force at moving velocity of 2 mm s^{-1}, 5.2% at 5 mm s^{-1} and 8.0% at 8 mm s^{-1}. Consequently, the guidance force is in positive correlation with the relative velocity between the PMG and the bulk superconductors.

To investigate this phenomenon, the YBaCuO bulk was simplified as a $R-L$ superconducting coil [24], with nonlinear resistance

$$L\frac{\mathrm{d}I}{\mathrm{d}t} + E_c \cdot \left(\frac{I}{I_c}\right) = -\frac{\partial \Phi}{\partial t}, \tag{1}$$

where L is the self-inductance based on its real geometry, t the time, I the flowing current in the superconductor and I_c is the critical current. E_c is a constant and Φ is the magnetic flux inside the coil produced by PMG:

$$\Phi = \int B\mathrm{d}A, \tag{2}$$

where B is the magnetic flux density produced by the PMG. A is the area of the coil. According to the Biot–Savart law, the element flux density dB can be described by

$$\mathrm{d}B = \frac{\mu_0}{4\pi} I' \frac{\mathrm{d}l \times \vec{r}}{r^2}, \tag{3}$$

where μ_0 is the permeability of vacuum and $\vec{r}$; is a coordinate vector from the element of length dl to the observation point, and I' is the magnitude of the current. The magnetic flux density can be calculated analytically [25]. And following equation (2), $\frac{\partial \Phi}{\partial t}$ can be expressed as

$$\frac{\partial \Phi}{\partial t} = \int \frac{\partial B}{\partial t}\mathrm{d}A = \int \frac{\partial B}{\partial y}\frac{\mathrm{d}y}{\mathrm{d}t}\mathrm{d}A = v \cdot \int \frac{\partial B}{\partial y}\mathrm{d}A. \tag{4}$$

Substituting equation (4) into equation (1), the current can be expressed as

$$I = ce^{-\frac{E_c t}{I_c L}} - v \cdot \frac{I_c \cdot \int \frac{\partial B}{\partial y}\mathrm{d}A}{Ec}, \tag{5}$$

where c is an integration constant which can be determined from the boundary conditions. When $t = 0$, v is equal to zero because the HTS bulks are rested in the equilibrium position; there is no induced current at this time, so $I = 0$. Substituting

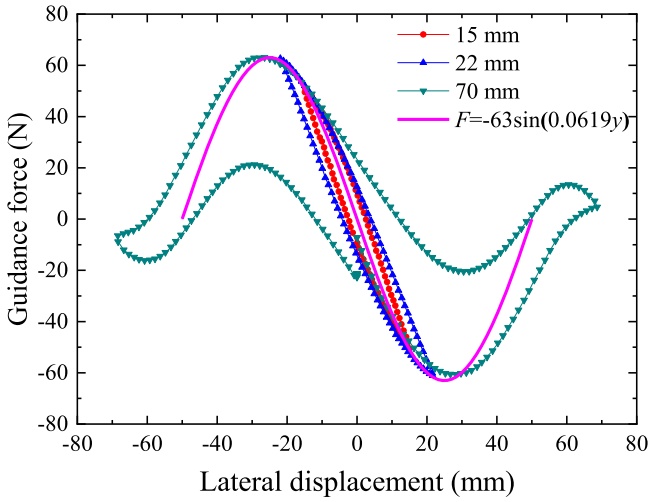

Figure 3. Guidance force curves of the HTS bulks at the chosen lateral displacement ranges of ±15 mm, ±22 mm and ±70 mm.

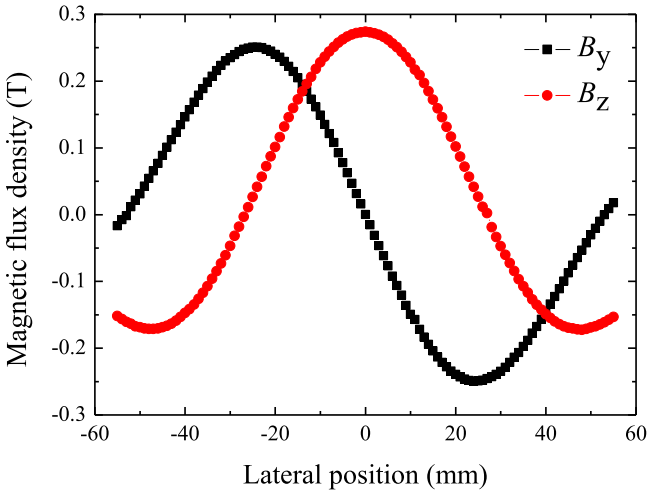

Figure 4. Magnetic flux density profiles of the applied PMG at a height of 15 mm. The PMG was schematically shown in figure 1(b).

the boundary conditions $v_{t=0} = 0$ and $I_{t=0} = 0$ into equation (5), we can deduce that $c = 0$. Hence, the guidance force can be expressed as

$$F_{Gui} = \int (I_y \times B_z)\, dA = -\int \left(v_y \cdot \frac{I_c \cdot \int \frac{\partial B}{\partial y} dA}{Ec} \right) \times B_z\, dA. \quad (6)$$

From the above equations, it can be qualitatively concluded that the guidance force is relative to the velocity. The greater the velocity, the greater the guidance force. The experimental results are qualitatively consistent with the theoretical analysis.

2.2.2. Guidance force versus lateral displacement. In this part, we fixed the relative moving velocity to 1 mm s^{-1}, and measured the hysteresis loops of the guidance force with largest lateral displacements of ±15 mm, ±22 mm and ±70 mm to study their dependence on the relative displacements. Displacement of 15 mm is measured as a reference, 22 mm usually the position where the largest guidance force appears, and 70 mm is the largest displacement we can achieve with the current setup. Figure 3 shows the guidance force curves in the various lateral displacement ranges. The guidance force curves in ranges of 15 mm and 22 mm present a similar trend. However, on increasing the displacement range to 70 mm, the hysteresis loop became significantly wide. It is considered that the restoring force has transformed from elastic deformation to elastic−plastic deformation [12]. Equation (6) reveals that guidance forces are generated by the interaction between the flux density of external magnetic field B and the current induced within the bulk superconductors. Figure 4 shows profiles of the vertical and lateral component of the magnetic flux density above the PMG at the height of 15 mm calculated by the method described in [25]. The profile of the flux density of the PMG is close to a sinusoid in both vertical and lateral directions. Coincidentally, the guidance force curve of 70 mm displacement range presents a sinusoid as well. We used a sine curve $F = -63\sin(0.0619y)$ to fit the guidance force curve as shown in figure 3 (pink). The fitting curve agrees well with the two guidance force curves with lateral ranges of 15 mm and 22 mm if the hysteresis of the guidance force is ignored. And the hysteresis of the guidance force will be taken into account in the next section.

Based on the above discussions, we can draw the conclusion that the guidance force is closely related to the relative velocity between the PMG and the HTS bulks; the guidance force curve can be approximately fitted by a sine curve. The specific fitting function will be discussed in the next section.

3. Simulation of lateral motion stability of the HTS maglev system

The obvious nonlinear hysteresis phenomenon was observed from the experiments described above, which is closely related to the dynamic stability of the HTS maglev system. In fact, the nonlinear hysteresis nature leads to complex long-term interaction between the HTS and PMG. Hence, a guidance force model describing the nonlinear hysteresis is required to investigate the dynamic behavior. In this part, we propose a mathematical model to analyze the nonlinear guidance force, and use it to further investigate the lateral motion stability of the HTS maglev system, which might represent the resistance ability to external excitations.

3.1. The nonlinear hysteretic model

According to dynamic responses, the model of the HTS maglev system can be described as

$$M[\ddot{y}] + C[\dot{y}] + K[y] = Q, \quad (7)$$

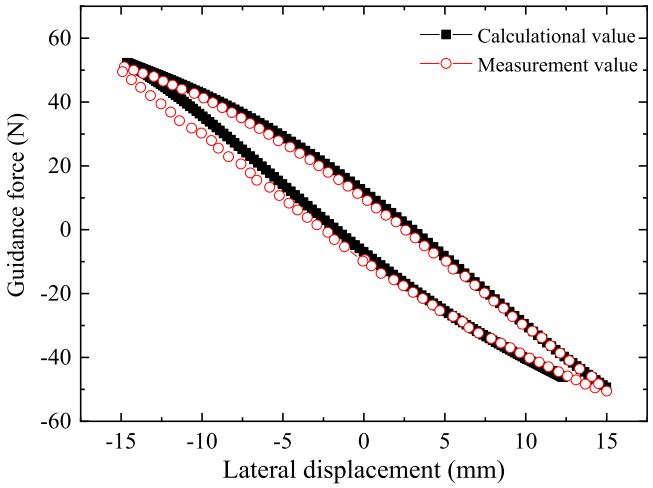

Figure 5. The experimental and simulated guidance force curves at a maximum lateral displacement of 15 mm.

where M, C, K and Q are mass matrix, damping matrix, stiffness matrix and excitation matrix respectively, while $[y]$ is the displacement vector, $[\dot{y}]$ the velocity vector and $[\ddot{y}]$ is the acceleration vector. As for the lateral motion of the HTS maglev system, the guidance force consists of ky and $c\dot{y}$. A new model of guidance force is presented as follows [26]:

$$F_{\text{gui}} = \alpha \sin(\beta y) + \eta_1 \dot{y} + \eta_2 \dot{y}^3. \tag{8}$$

The model is composed of two parts, where $\alpha \sin(\beta y)$ is the basis function (where α reflects the maximum guidance force and β reflects the wavelength of the guidance force). This part is close to the fitting curve $F = -63\sin(0.0619y)$ shown in figure 3. The other part $\eta_1\dot{y} + \eta_2\dot{y}^3$ represents the linear and nonlinear parts of damping. Where $\alpha = -63$ is certain by the amplitude of the fitting curve. The other three parameters β, η_1 and η_2 are determined by the means of parameter identification through comparison with experimental data. The parameters of equation (8) are listed in table 2.

Substituting the parameters listed in table 2 into equation (8), it can be solved by the Runge–Kutta method. The initial value is $y = 15$ mm and $\dot{y} = 0$ m s^{-1}. The displacement $y(t_i)$ and the velocity $\dot{y}(t_i)$ can be obtained. Where $f(t_i)$ represents a function of discrete time. The guidance force $F_{\text{gui}}(t_i) = \alpha \sin(\beta y(t_i)) + \eta_1 \dot{y}(t_i) + \eta_2 \dot{y}(t_i)^3$ can also be obtained. Figure 5 shows the comparison between the calculated curve and the experimental curve of the guidance force at a measurement scale of 15 mm. The black solid line shown in figure 5 is the calculated $F_{\text{gui}}(t_i) \sim y(t_i)$ curve. The calculated curve matches the measured results well. It reproduces the hysteresis features, and the amplitudes are almost the same. The main distinction between these two curves is that the calculated curve is not closed, because there exists energy loss in the simulation due to the hysteresis (this can be thought of as the damping in dynamics), and it cannot return to its initial position having experienced a period of free motion.

Table 2. Values of parameters in equation (8).

α	β	η_1	η_2
−63	0.066 84	−2	−350

3.2. Lateral motion stability

Because of the obviously nonlinear nature of the guidance force, the lateral motion stability, which is closely related to the safety of the vehicle, becomes particularly important. Study of the motion stability is required to clarify the behaviors under external disturbance or shock. In this part, we will address the lateral motion stability of the HTS maglev system by simulation.

Combining equations (7) and (8), the lateral motion equation can be written as:

$$m\ddot{y} - \alpha \sin(\beta y) - \eta_1 \dot{y} - \eta_2 \dot{y}^3 = 0. \tag{9}$$

For a convenient solution, the second order differential equation (9) is transformed into two first order ordinary differential equations (10) through a simple transform $y_1 = y$, $y_2 = \dot{y}$. In equation (10), y_1 represents the displacement and y_2 represents the velocity.

$$\left.\begin{aligned} \dot{y}_1 &= f_1(y_1, y_2) = y_2 \\ \dot{y}_2 &= f_2(y_1, y_2) = (\alpha \sin(\beta y_1) + \eta_1 y_2 + \eta_2 {y_2}^3)/m \end{aligned}\right\}. \tag{10}$$

Equation (10) is a typical nonlinear system; the stability of a nonlinear system can be characterized by analyzing the stability of its corresponding linearized system according to the linear stability theorem as follows:

1. If the fixed point of the linearized system is asymptotically stable, the corresponding reference point of the nonlinear system is an asymptotically stable solution.
2. If the fixed point of the linearized system is unstable, the corresponding reference point of the nonlinear system is an unstable solution.

So, the nonlinear system equation (10) is rewritten as equation (11) based on Taylor's theorem:

$$\dot{\boldsymbol{y}} = D\boldsymbol{y} + R(\boldsymbol{y}); \quad \|R(\boldsymbol{y})\| = o(\|\boldsymbol{y}\|), \tag{11}$$

where

$$\left.\begin{aligned} D &= \frac{\partial f}{\partial y} = \begin{bmatrix} \dfrac{\partial f_1(y)}{\partial y_1} & \dfrac{\partial f_1(y)}{\partial y_2} \\ \dfrac{\partial f_2(y)}{\partial y_1} & \dfrac{\partial f_2(y)}{\partial y_2} \end{bmatrix}; \\ \|R(\boldsymbol{y})\| &= o(\|\boldsymbol{y}\|); \quad \lim_{\|\boldsymbol{y}\|\to 0} \frac{\|R(\boldsymbol{y})\|}{\|\boldsymbol{y}\|} = 0 \\ \boldsymbol{y} &= \begin{pmatrix} y_1 \\ y_2 \end{pmatrix}; \quad \dot{\boldsymbol{y}} = \begin{pmatrix} \dot{y}_1 \\ \dot{y}_2 \end{pmatrix} \end{aligned}\right\}. \tag{12}$$

In equation (11), $D\boldsymbol{y}$ is the linear term and $R(\boldsymbol{y})$ is the high order perturbation. So the corresponding linearization equations can be written as

$$\dot{\boldsymbol{y}} = D\boldsymbol{y}, \tag{13}$$

where D is called the linearized Jacobian matrix.

According to the linear stability theorem, the stability of the nonlinear system equation (10) can be found by analyzing the stability of its corresponding linearized system equation (13). Firstly, the fixed points are located by solving

$$\dot{\boldsymbol{y}} = D\boldsymbol{y} = 0. \tag{14}$$

The parameters used in equation (14) are listed in table 2, and m = 3.5 kg.

Three families of equilibrium solutions are obtained by solving equation (14). That means there are three singular points in the lateral motion of the HTS maglev system, which are $\begin{cases} y_1 = 0 \\ y_2 = 0 \end{cases}$, $\begin{cases} y_1 = 0.047 \\ y_2 = 0 \end{cases}$ and $\begin{cases} y_1 = -0.047 \\ y_2 = 0 \end{cases}$. The motion stability criteria can then be used to analyze the motion stability [27].

Motion stability criteria: As for the linear dynamical system (13),

1. If all of the eigenvalues of D have negative real part, the system is asymptotically stable.
2. If one or more eigenvalues have positive real part, the system is unstable.
3. If some of the eigenvalues have zero real part whereas the rest have negative real part, the singular point is defined asnon-hyperbolic, and its motion stability requires further discussion.

For the singular point (0, 0),

$$D_{(0,0)} = \begin{pmatrix} 0 & 1 \\ \alpha\beta & \eta_1 \end{pmatrix}, \tag{15}$$

$$\det(D - \lambda E) = \lambda^2 - \eta_1\lambda - \alpha\beta = 0, \tag{16}$$

where E is the identity matrix. By solving equation (16), the eigenvalues are

$$\lambda = -1 \pm 65i. \tag{17}$$

All of the eigenvalues have a negative real part. According to the motion stability criteria, the system is asymptotically stable in the neighborhood of (0, 0), and (0, 0) is a stable focus point.

For the singular points (±0.047, 0),

$$D_{(\pm 0.047,0)} = \begin{pmatrix} 0 & 1 \\ -\alpha\beta & \eta_1 \end{pmatrix}, \tag{18}$$

$$\det(D - \lambda E) = \lambda^2 - \eta_1\lambda + \alpha\beta = 0. \tag{19}$$

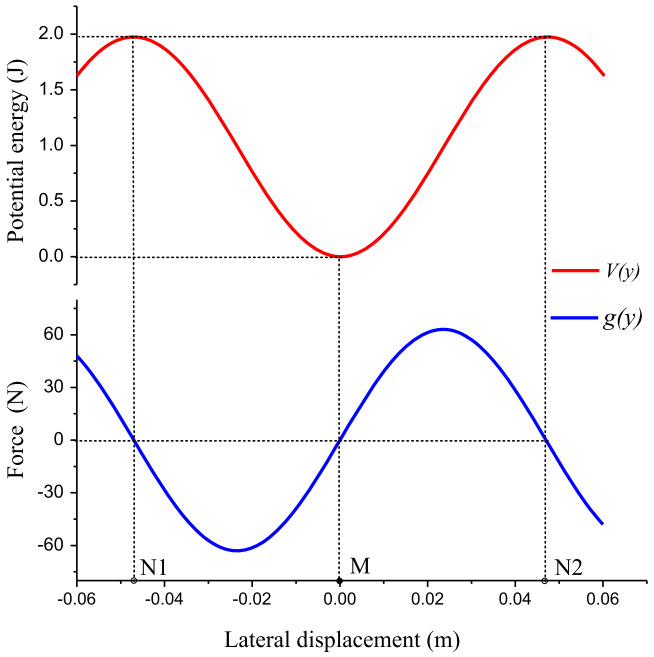

Figure 6. The graphs of $g(y)$ and $V(y)$. There are three singular points in the system, N1 (−0.047) and N2 (0.047) are unstable, and M (0) is stable.

By solving equation (19), the eigenvalues are

$$\lambda_1 = 64, \quad \lambda_2 = -66. \tag{20}$$

So, one of the eigenvalues has a positive real part. According to the motion stability criteria, the system is unstable in the neighborhood of (±0.047,0) and both the two singular points are unstable saddles.

Another intuitive way to estimate the motion stability is to draw the potential energy function of the corresponding undamped system. The corresponding undamped system of equation (9) is

$$m\ddot{y} - \alpha \sin(\beta y) = 0. \tag{21}$$

Let $g(y) = -\alpha \sin(\beta y)$, which is called the generalized force function. Let $V(y) = -\int g(y)\mathrm{d}y = \int \alpha \sin(\beta y)\mathrm{d}y = -\frac{\alpha}{\beta}\cos(\beta y)$ and $V(0) = 0$. $V(y)$ is called the potential energy function. The graphs of $g(y)$ and $V(y)$ are shown in figure 6. There are three zeros for $g(y)$ corresponding three extreme values of the function of potential energy function. When y = ±0.047, $V(y)$ has the local maximum which means the points are unstable. When y = 0, $V(y)$ has the local minimum which means the point is stable.

The stability of the three singular points has been investigated using the two methods mentioned above, and the results are the same. They are a stable focus point and two unstable saddle points. In order to understand the lateral motion stability throughout the region, the lateral motion phase portrait of the HTS maglev system was drawn by Matlab, as exhibited in figure 7. Calculation results verify the existence of one stable focus and two unstable saddle points. There are infinite numbers of solutions for equation (10) with different initial conditions. But the solutions can be divided

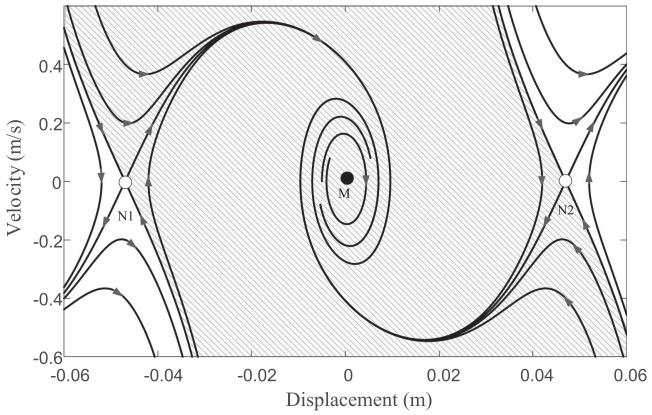

Figure 7. The phase portrait of lateral motion of the HTS maglev system. The singular point M is a stable focus around which all the trajectories will fall on it. The singular points N_1 and N_2 are saddle points which distinguish the stable and unstable regions.

into two categories: in or out of the shaded area. Those solutions in the shaded area converge to the equilibrium position over time, but those outside cannot.

In figure 7, M (0, 0), N_1 (−0.047, 0) and N_2 (0.047, 0) are the three singular points in the lateral motion of the HTS maglev system, and are consistent with those in figure 6. M is a stable focus point around which the points in the stable region will flow to point M at the end of the lateral motion. This is the phenomenon of 'self-stability' [1]. The other two singular points (N_1 and N_2) are unstable saddle points, which means the vehicle can only theoretically remain at the equilibrium position without disturbance. When disturbance exists, it is possible for the vehicle to enter either the stable or unstable region. The phase plane can be divided into two kinds of region: the stable region (shaded) and unstable region (unshaded). The vehicle will eventually come back to the equilibrium position if it runs in the stable region, and will derail or even overturn if the motion of the vehicle enters the unstable region.

4. Conclusion

To understand the complex dynamic behavior of HTS maglev systems, we measured the guidance force at various velocities and movement ranges. A nonlinear hysteretic model, based on the experimental data, was proposed to describe the hysteretic character of the guidance force. The model was then extended—equation (8)—to simulate the lateral motion, and to verify its stability. Based on the studies mentioned above, conclusions can be drawn as follows:

(1) The guidance force, as demonstrated by the experimental results, is proportional to the relative velocity of bulk superconductors to the PMG.
(2) The proposed hysteretic nonlinear model reproduced the hysteretic character of the guidance force due to the HTS bulk superconductors, and describes the relationship between the guidance force and the movement velocity well.
(3) Three singular points, one stable focus point and two unstable saddle points, have been found in the lateral motion of the HTS maglev. The phase diagram can thus be divided into two regions, a stable region and an unstable region. The vehicle will eventually come back to the stable equilibrium position if it runs in the stable region, but not in the unstable region.

Acknowledgments

This work was partially supported by the the Science and Technology Partnership Program, Ministry of Science and Technology of China, the Fundamental Research Funds for the Central Universities (2682018ZT22 and 2682018CX72) and the Foundation of Key Laboratory of Magnetic Suspension Technology and Maglev Vehicle, Ministry of Education.

ORCID iDs

Zigang Deng https://orcid.org/0000-0001-7937-9081
Jun Zheng https://orcid.org/0000-0002-8493-0592

References

[1] Brandt E H 1989 Levitation in physics *Science* **243** 349–55
[2] Wang J S *et al* 2002 The first man loading high temperature superconducting maglev test vehicle in the world *Physica* C **378-381** 809–14
[3] Schultz L *et al* 2005 Superconductively levitated transport system—the supratrans project *IEEE Trans. Appl. Supercond.* **15** 2301–5
[4] Sotelo G G *et al* 2015 A full scale superconducting magnetic levitation (maglev) vehicle operational line *IEEE Trans. Appl. Supercond.* **25** 3601005
[5] Deng Z *et al* 2016 A high-temperature superconducting maglev ring test line developed in Chengdu, China *IEEE Trans. Appl. Supercond.* **26** 3602408
[6] Cai Y and Rote D M 2002 Review of dynamic stability of repulsive force maglev suspension systems *IEEE Trans. Magn.* **38** 1383–90
[7] Deng Z *et al* 2007 Free vibration of the high temperature superconducting maglev vehicle model *IEEE Trans. Appl. Supercond.* **17** 2071–4
[8] Moon F C, Yanoviak M M and Ware R 1988 Hysteretic levitation forces in superconducting ceramics *Appl. Phys. Lett.* **52** 1534–6
[9] Hikihara T and Moon F C 1994 Chaotic levitated motion of a magnet supported by superconductor *Phys. Lett.* A **191** 279–84
[10] Alloui L *et al* 2013 Numerical study of the relation between the thermal effect and the stability of the levitation system excited by an external source *Physica* C **487** 1–10
[11] Zheng J *et al* 2007 Stability of the maglev vehicle model using bulk high Tc superconductors at low velocity *IEEE Trans. Appl. Supercond.* **17** 2103–6
[12] Wang X R *et al* 2003 Levitation force and guidance force of bulk in applied field *Physica* C **386** 536–9
[13] Riise A B, Johansen T H, Bratsberg H and Yang Z J 1992 Logarithmic relaxation in the levitation force in a magnet–high Tc superconductor system *Appl. Phys. Lett.* **60** 2294–6

[14] Gou X F, Zheng X J and Zhou Y H 2007 Drift of levitated/suspended body in high-Tc superconducting levitation systems under vibration—part II: drift velocity for gap varying with time *IEEE Trans. Appl. Supercond.* **17** 3803–8
[15] Zhuo P J, Zhang Z X and Gou X F 2016 Chaotic motion of a magnet levitated over a superconductor *IEEE Trans. Appl. Supercond.* **26** 1–6
[16] Hull J R 2000 Superconducting bearings *Supercond. Sci. Technol.* **13** R1–15
[17] Moon F C 1988 Chaotic vibrations of a magnet near a superconductor *Phys. Lett.* A **132** 249–52
[18] Sugiura T, Tashiro M, Uematsu Y and Yoshizawa M 1997 Mechanical stability of a high-Tc superconducting levitation system *IEEE Trans. Appl. Supercond.* **7** 386–189
[19] Ma G T, Wang J S and Wang S Y 2011 Numerical study of the speed-related behavior of the magnetic force in the HTS maglev system based on a 3D model *J. Supercond. Nov. Magn.* **24** 1593–8
[20] Li J *et al* 2017 Nonlinear vibration behaviors of high-Tc superconducting bulks in an applied permanent magnetic array field *J. Appl. Phys.* **121** 243901
[21] Navau C, Sanchez A and Pardo E 2003 Lateral force in permanent magnet-superconductor levitation systems with high critical current *IEEE Trans. Appl. Supercond.* **13** 2185–8
[22] Qin M J *et al* 2002 Calculation of the hysteretic force between a superconductor and a magnet *Phys. Rev.* B **66** 81–8
[23] Wang J S *et al* 2000 High Tc superconducting magnetic levitation measurement system *High Technol. Lett.* **10** 55–8 (in Chinese)
[24] Postrekhin E *et al* 2001 Dynamics and relaxation of magnetic stress between magnet and superconductor in a levitation system *IEEE Trans. Appl. Supercond.* **11** 1984–7
[25] Gou X, Yang Y and Zheng X 2004 Analytic expression of magnetic field distribution of rectangular permanent magnets *Appl. Math. Mech.* **25** 297–306
[26] Cheng X W and Wei H 2015 Research status of hysteretic nonlinear mode *China Acad. J. Electron. Publ. House* **02** 184–7 (in Chinese)
[27] Nayfeh A H and Balachandran B 1995 *Applied Nonlinear Dynamics: Analytical, Computational, and Experimental Methods* (New York: Wiley)